RESEARCH ARTICLE

Crystal Structure of the Potassium Channel KirBac1.1 in the Closed State

Anling Kuo,[1] Jacqueline M. Gulbis,[2] Jennifer F. Antcliff,[3] Tahmina Rahman,[1] Edward D. Lowe,[1] Jochen Zimmer,[1] Jonathan Cuthbertson,[1] Frances M. Ashcroft,[3] Takayuki Ezaki,[4] Declan A. Doyle[1]*

The KirBac1.1 channel belongs to the inward-rectifier family of potassium channels. Here we report the structure of the entire prokaryotic Kir channel assembly, in the closed state, refined to a resolution of 3.65 angstroms. We identify the main activation gate and structural elements involved in gating. On the basis of structural evidence presented here, we suggest that gating involves coupling between the intracellular and membrane domains. This further suggests that initiation of gating by membrane or intracellular signals represents different entry points to a common mechanistic pathway.

K^+ channels are involved in a wide range of physiological processes, such as propagation of the action potential, cardiac function, K^+ reabsorption in the kidney, and hormone regulation (*1*, *2*). This diversity is possible because many different signals can open or close K^+ channels, a process known as gating. The signals are received by domains attached to the pore-forming subunit.

We present a complete K^+ channel structure that shows the nature of the physical link coupling domains that receive gating signals to the transmembrane helices. We identify residues that form the activation gate and propose a mechanism for gating and domain coupling. We also describe the process of rectification at the molecular level and outline additional means by which Kir channels block ion movement through the ion-conduction pathway in the closed state.

Description of the KirBac1.1 structure. Recognition that inwardly rectifying K^+ channels occur in prokaryotic genomes allowed for the production of the channel in sufficient quantities for crystallization trials (*3*). One suitable crystal form allowed structure determination to a resolution limit of 3.65 Å with a final *R* factor of 0.295 (Table 1). The crystallographic model is complete over all regions, excluding two loops (residues 196 to 205 and residues 290 to 295) and the N (1 to 35) and C termini (310 to 331), which were insufficiently ordered to build into the electron density maps (fig. S1) (*4*).

The KirBac1.1 structure consists of an all α-helical integral membrane section plus an intracellular domain consisting mostly of β sheet (Fig. 1). The potential total distance that an ion must travel as it passes through the channel from the extracellular turret to the bottom of the C-terminal domain is 88 Å. It is substantially longer than the predicted distance of 64 Å, based on the crystal structure of the homologous intracellular GIRK (G-protein–coupled inwardly rectifying K^+ channel) domain of Kir3.1 (*5*). The maximum and minimum outer diameters, perpendicular to the ion-conduction pathway, are 54 and 43 Å for the transmembrane section and 78 and 50 Å for the C-terminal domains. In accordance with nomenclature describing the KcsA structure (*6*), the membrane helices are labeled inner, outer, and pore helix (Fig. 1 and fig. S2). An extra helix named the slide helix is present in the transmembrane section of the KirBac1.1 structure. This amphipathic helix runs parallel with the membrane/cytoplasmic interface. A similar arrangement for the N-terminal helix of KcsA was determined from spin labeling electron paramagnetic resonance measurements (*7*).

KirBac1.1 can be divided structurally into five regions. On the extracellular side is the selectivity filter followed by a cavity, gate, flexible linkers, and cytoplasmic vestibule (Fig. 1). The linkers connecting the inner and outer helices to the N- and C-terminal domains are fully resolved in the crystal structure. We believe it is unlikely that K^+ ions enter the channel through gaps between the linkers owing to the presence of positively charged arginine and lysine residues (residues 151 to 155) that repel cations (Fig. 2A). Three N-terminal residues (40 to 42) interact with a β strand (residues 298 to 300) on the outer edge of the C-terminal domain (Fig. 2B and Fig. 5A), forming a small parallel β sheet. A similar interaction is seen in the crystal structure of the fused intracellular N- and C-terminal domains of the Kir3.1 channel (*5*); however, in the complete channel structure the N terminus interacts with the C-terminal domain from the adjacent subunit. Flexible linkers (residues 150 to 153) connect the inner helix covalently to the C-terminal domain.

Kir family of potassium channels. Agreement of the KirBac1.1 structure with structurally derived information from Kir channels and sequence alignments demonstrates that KirBac1.1 is a structural representative of the eukaryotic Kir channel family. Random mutagenesis of the inner and outer helices of Kir2.1 identified restricted residues that were not amenable to change (*8*). Mapping the restricted residues (Fig. 2C, red and purple resi-

Table 1. Crystallographic structure determination and refinement. rms, root mean square.

Data set	Sites	Resolution (Å)	Reflections (measured/unique)	Completeness (%) (overall/outer shell)	R_{merge} (%)* R_{iso}† (overall/outer shell)
Native1 Data		28.8–3.80	37,109 /12,005	94.1/89.9	0.096/0.327
Native2 Data		20.0–3.65	87,944/14,455	100.0/99.4	0.087/0.412
Thimerosal T128C	2	37.8–4.0	44,538/8,455	75.0/70.5	0.057/0.216
Thimerosal A125C	2	20.0–4.0	36,000/10,783	98.7/98.7	0.081/0.395
RbCl	4	27.6–4.0	27,384/9,546	87.4/76.7	0.108/0.273

Refinement statistics					rms deviations	
Data	Resolution (Å)	R_{free}	R_w	No. reflections (all/working/free)	Bond lengths (Å)	Bond angles (°)
Native2	7.5–3.65	0.329	0.295	12,773/12,135/638	0.017	2.0

*$R_{merge} = \Sigma\Sigma|I_j - \langle I \rangle|/\Sigma I_j$. †$R_{iso} = \Sigma|F_P - F_{PH}|/\Sigma F_P$.

[1]University of Oxford, Department of Biochemistry, Laboratory of Molecular Biophysics, South Parks Road, Oxford OX1 3QU, UK. [2]Structural Biology Division, The Walter and Eliza Hall Institute of Medical Research, [1]G Royal Parade, Parkville, Victoria 3050, Australia. [3]University of Oxford, University Laboratory of Physiology, Parks Road, Oxford OX1 3PT, UK. [4]Department of Microbiology and Bioinformatics, Gifu University Graduate School of Medicine, Regeneration, and Advanced Medical Science, 40 Tsukasamachi, Gifu 500-8705, Japan.

*To whom correspondence should be addressed. E-mail: declan@biop.ox.ac.uk

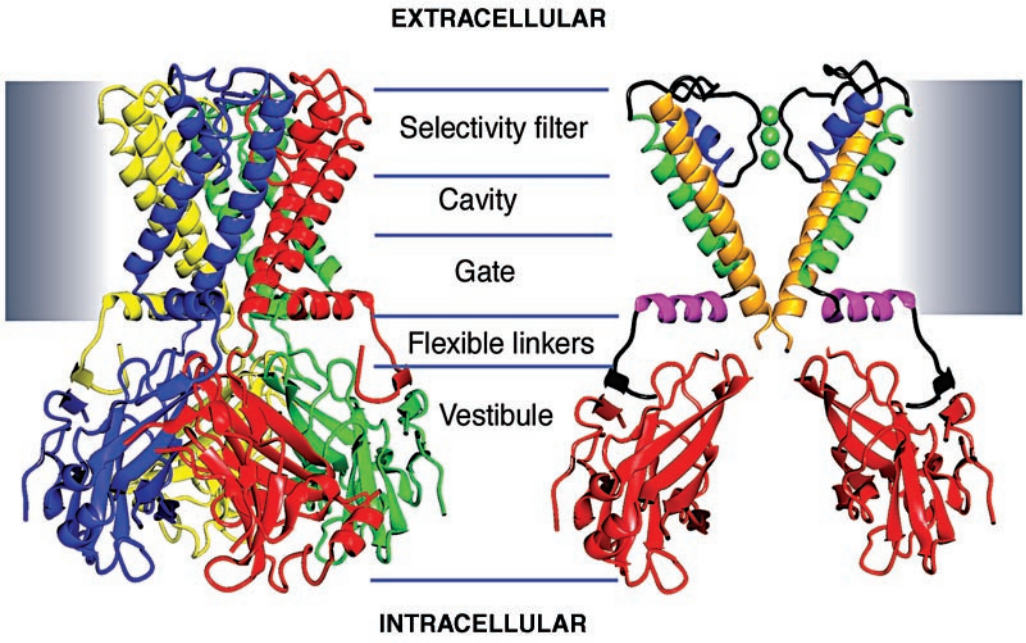

Fig. 1. Overview of the KirBac1.1 structure. The position of the membrane is represented by the shaded bar. On the left, monomers are individually colored to highlight the relative orientation of secondary structural elements and domains. On the right, two monomers have been removed for clarity so that the positions of the following structural elements can be seen: slide helix (pink), outer helix (green), pore helix (blue), inner helix (yellow), and C-terminal domain (red).

dues) onto the KirBac1.1 structure indicates that they play an important role in protein-protein contacts around the selectivity filter. There is also excellent agreement for variable residues (yellow residues) that face the lipid membrane and residues that form and line the cavity (cyan residues). In another set of experiments, amino acids on the inner helix of Kir6.2 were systematically substituted with cysteine, allowing the accessibility of each mutated residue to be assessed by the application of cadmium ions (*9*). On this basis, it was proposed that the three most Cd^{2+}–reactive residues (Leu^{164}, Phe^{168}, and Ala^{172}) line the ion-conduction pathway. The structure confirms that equivalent residues in the KirBac1.1 sequence (Thr^{142}, Phe^{146}, and Ala^{150}) form part of the ion-conduction pathway (Fig. 2C).

Dimer-of-dimers. An ion-conduction pathway forms at the common interface between all four subunits of a K^+ channel. In our crystals, the conduction pathway of the channel is colinear with a crystallographic two-fold axis. Each asymmetric unit of the crystal contains two subunits, related to a second pair by a simple two-fold rotation. The transmembrane and intracellular domains of the channel are hinged with respect to one another at the cytosolic face of the membrane. Although the transmembrane section displays four-fold symmetry, the intracellular domains are in a two-fold arrangement.

Rectification. Inwardly rectifying K^+ channels act as diodes or valves allowing current to flow preferentially inward. The KirBac1.1 crystals were grown in the presence of Mg^{2+} ions. Mg^{2+} ions and polyamines produce current rectification by directly blocking K^+-ion flow. The residues shown to be important in rectification in Kir2.1 and Kir1.1 are equivalent to residues Ile^{138}, Glu^{187}, and Glu^{258} in KirBac1.1 (*10*–*14*). Glu^{187} and Glu^{258} form part of the C-terminal vestibule's lining (Fig. 3). In all four subunits of KirBac1.1, the glutamate side chains point to the center of the ion-conduction pathway, forming a double ring of negatively charged residues, where the Glu^{187}

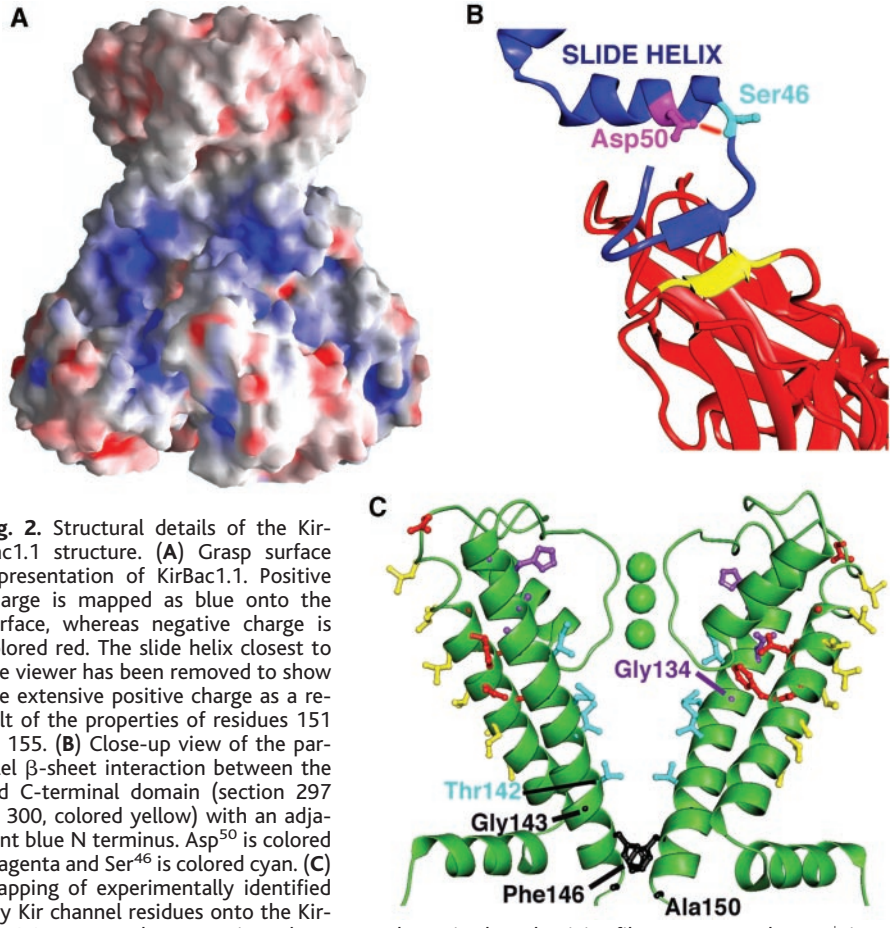

Fig. 2. Structural details of the KirBac1.1 structure. (**A**) Grasp surface representation of KirBac1.1. Positive charge is mapped as blue onto the surface, whereas negative charge is colored red. The slide helix closest to the viewer has been removed to show the extensive positive charge as a result of the properties of residues 151 to 155. (**B**) Close-up view of the parallel β-sheet interaction between the red C-terminal domain (section 297 to 300, colored yellow) with an adjacent blue N terminus. Asp^{50} is colored magenta and Ser^{46} is colored cyan. (**C**) Mapping of experimentally identified key Kir channel residues onto the KirBac1.1 transmembrane section. The green spheres in the selectivity filter represent three K^+ ions.

ring is farther from the membrane. The potential negatively charged ring when a glutamate side chain is present at position 138 is also highlighted in Fig. 3. The distance between position 138 and Glu^{258} is ~35 Å, too long for a single spermine molecule (~20 Å long) to overlap with both sites.

Electrostatic rings of negative charge also affect ion conduction in channels such as the acetylcholine receptor (AChR), which has three negatively charged electrostatic rings (*15*). As with the Kir2.1 channel (*12*), these electrostatic rings enhance ion conduction.

The kinetics of blocking by Mg^{2+} and polyamines differ. Mg^{2+} displays faster on-off kinetics. The slower component of rectification is produced by endogenous polyamines that have a higher affinity than Mg^{2+} ions (*16*–*18*). Polyamines are linear molecules with evenly spaced positive charges. Study of Mg^{2+} and polyamine interactions with anion binding sites gives insight into their differing binding properties (*19*). The major points are as follows: (i) binding of Mg^{2+} is stronger than that for polyamines if the anion binding site is highly charged and confined; (ii) this preference is reversed if the anionic charge is spread out; and (iii) if the charges are spread out, matching of charges becomes a priority. Therefore, the shape, charge, and hydrophobicity of the polyamine determine its binding affinity. This is consistent with the architecture seen in Kirbac1.1, in which the two anionic charged rings are spread out and the side chains of Glu^{187} and Glu^{258} are ~8 Å away from their nearest glutamate neighbor. These outstretched negatively charged glutamate rings suggest that coordination of linear positively charged polyamines is favored over that of compact Mg^{2+} ions.

The closed state. During the process of rectification, the flow of K^+ ions from a cell is temporarily blocked by Mg^{2+} or polyamines. This is not the same as the channel's being closed. Reversal of the applied voltage or an increase of the external K^+ concentration can remove the block. This channel is in the closed state because the ion-conduction pathway is blocked by the side chains of Phe^{146}. We call this amino acid the "blocking residue" for structural reasons, but it is likely to be the "activation gate" in electrophysiological terms (Fig. 2C and Fig. 4A). The sequence alignment of Kir channels indicates that residues with large hydrophobic aromatic or aliphatic side chains are favored in this position (fig. S2).

The first structural evidence of the use of hydrophobic residues to block an ion-conduction pathway was described by Unwin for the AChR (*20*, *21*). Structures of the AChR in an open and closed state showed that the hydrophobic leucine side chains rotate into the center of the ion-conduction pathway in the closed state. For the mechanosensitive ion channel MscL, two residues, isoleucine and valine in a pentameric arrangement, form another hydrophobic constriction within the transmembrane section of its ion-conduction pathway (*22*). Molecular dynamics simulations of a model channel indicate that a hydrophobic-lined pore acts as an effective gate preventing water and ion movement (*23*). The exact configuration of the pore was critical in determining this effectiveness. This is reflected in the different configurations of the ion-conduction pathways of the AChR, MscL, and KirBac1.1, but they all appear to make use of hydrophobic residues to block water and therefore ion movement.

Another feature of the closed state is that the pore helices no longer point directly at the center of the channel cavity, unlike KcsA (Fig. 4B). The C termini of the pore helices of KcsA point toward the center of the cavity, focusing a cation in the center (*6*). In the closed KirBac1.1 channel, the four pore helices are misaligned. Because 80% of the energy of ion stabilization in the cavity is derived from the pore-helix dipoles (*24*), loss of the combined dipole effect may result in destabilization of the ion in the center of the cavity. In contrast to KcsA, weak, broken electron density is present in this area. The formation of the KirBac1.1 closed state also results in a decrease in the volume of the cavity. The decreased volume accommodates fewer water molecules (27 in KcsA and 20 in KirBac1.1), which is also likely to destabilize an ion in this region.

The conformation of the pore helices implies that the selectivity filter of KcsA is in an open state. We hypothesize that the truncated KcsA crystal structure represents an open channel that has a closed gating section.

The selectivity filter. In the closed KirBac1.1 structure there are only three K^+

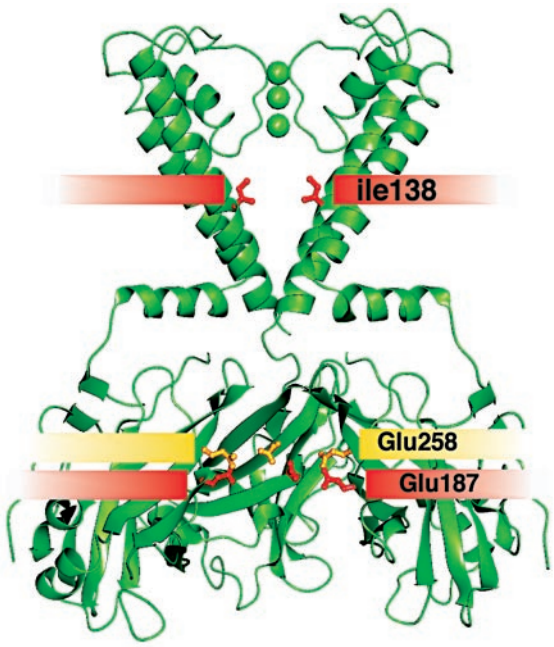

Fig. 3. Rings of electrostatic charge are a feature of Kir channels. The transmembrane sections closest to and farthest from the viewer have been removed. For the C-terminal domains, only the closest domain to the viewer has been removed. The C-terminal domain negatively charged rings Glu^{258} and Glu^{187} are highlighted in yellow and red, respectively. The likely position of a third charged ring at position Ile^{138} is also highlighted in red.

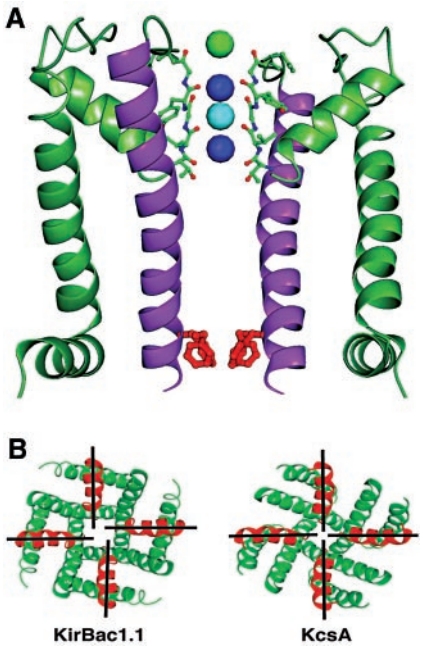

Fig. 4. Conformation of the selectivity filter and the pore helices. (**A**) Ribbon representation of the transmembrane section of two opposing KirBac1.1 monomers. The structure has been rotated ~80° from the viewing position in Fig. 1. The residues forming the selectivity filter, displayed as ball-and-stick, interact with four K^+ ions, colored green (S_{ext}), indigo (S_1), cyan (S_2), and indigo (S_3). The inner helices are colored purple, whereas the side chains of the Phe^{146} blocking residues are colored red. (**B**) Relative positions of the pore helices are depicted in red in the crystal structure of KirBac1.1 and KcsA. This view is from the extracellular side of the channel looking directly down the central ion-conduction pathway. Black lines through the center of each pore helix indicate its orientation relative to the center of the cavity.

binding sites within the selectivity filter: S_1, S_2, and S_3 (Fig. 4A). In a 2.0 Å KcsA structure where crystals were grown in 200 mM KCl (high K^+), an extra K^+ binding site (S_4) is present (*25*). Both KcsA and KirBac1.1 have an extracellular K^+ binding site (S_{ext}). What we observe in the filter is likely to be an averaged view of alternate configurations, i.e., in some channels the filter contains a single K^+ ion (S_2) and in others it contains two K^+ ions (S_1 and S_3). The S_2 binding site is in the middle of the filter, whereas the S_1 and S_3 binding sites are equidistant from either end. The temperature factor, B_{iso}, reflects the ions' mobility. In the high-K^+ structure, which represents the open state of the selectivity filter, the temperature factors are approximately equal for all four ions. In the KirBac1.1 closed configuration, the temperature factor for the S_2 K^+ ion is lower than that for the S_1 and S_3 ions (B_{iso} = 5, 23, and 58 Å^2, respectively), which indicates that this is a stable conformation of the selectivity filter. A second high-resolution KcsA structure, with crystals grown in 3 mM KCl (low K^+), produced a constriction in the center of the filter (*25*). This filter conformation was thought to represent a nonconducting form. The low-K^+ filter conformation has a constriction that maps directly to the S_2 ion position in KirBac1.1. This ion position probably prevents the KirBac1.1 filter from collapsing. The movement of the KirBac1.1 channel into a closed state has essentially preserved the open-state architecture of the filter. On this basis we propose that the selectivity filter of KirBac1.1 is in a protected state that, although not allowing ion flow, maintains a conformation that prevents collapse. Hence the filter is poised to move into an active, open conformation when required.

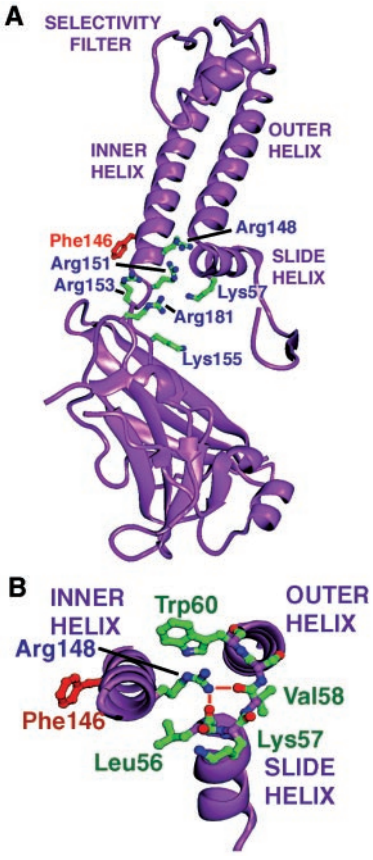

Fig. 5. Detail showing important residues at the transmembrane/C-terminal domain interface. (**A**) A single complete monomer colored purple is shown. Several positively charged arginine and lysine residues cluster at the interface, preventing cations from entering the ion-conduction pathway between the linkers. (**B**) Detail of the Arg^{148}–slide helix interaction viewed from the intracellular side of the membrane looking along the inner and outer helices. Figures 1 to 5 were produced with the program Aesop (*29*).

Gating hypothesis. For KirBac1.1 to open, the pore helices must move away from their positions in the closed state. Structural elements likely to be involved include slide helix, outer helix, inner helix, flexible linkers (Fig. 5A, residues 150 to 153), and the N-, C-terminal domain interaction. Figure 5B shows an important interaction between the slide helix and the conserved Arg^{148} (fig. S2). The positively charged arginine side chain interacts with the negative, C-terminal end of the slide helix. This is another example of nature using helix dipoles in K^+ channels. In addition, there is an interaction between the C-terminal domain (residues 298 to 300) and N-terminal residues 40 to 42 of an adjacent subunit (Fig. 2B). The N-terminal strand is attached to the slide helix by a short, extended polypeptide (residues 43 to 47). A conserved aspartate (Asp^{50}) on the slide helix stabilizes this connection by hydrogen bonding to the backbone nitrogen of Ser^{46} (Fig. 2B).

The nature of the intracellular domain movement during gating is not known; however, it must result in the blocking residue moving away from its position in the closed state. A hypothesis is shown schematically in Fig. 6. An outward rotation of the intracellular domains would draw the bottom of the inner helix away from the center of the ion-conduction pathway. The slide helices move laterally, resulting in displacement of the outer helices, which allows room for the inner helices to bend.

Inner-helix bending. The most likely position for a helix to bend is at a point of weakness. Glycine and proline residues promote distortions of transmembrane helices (*26*). Kirbac1.1 has glycine residues at positions 134, 137, and 143 of the inner helix. Of these glycine residues, only Gly^{143} is highly conserved among Kir channels (fig. S2). In contrast, the MthK hinge region is Gly^{83} (*27*), the equivalent of Gly^{134} in KirBac1.1. This position should be highly conserved if it is the hinge region for all K^+ channels. Sequence alignments show that this glycine is not fully conserved. The equivalent of Gly^{134} in Kir2.1 is one of the restricted residues involved in protein packing (Fig. 2C). This implies that in Kir channels the Gly134 position is probably more important in protein packing than it is in gating. For KirBac1.1 and by extension all other Kir channels, small side-chain residues at position 134 allow the inner helix to bend after it has passed the selectivity-filter section. The inner helices of KirBac1.1 bend by ~12° as they pass the selectivity filter (purple inner helix in Fig. 4A).

In the voltage-dependent Shaker K^+ channel, two proline residues (Pro^{473} and Pro^{475}) form part of the inner helix. Pro^{475} is in alignment with Gly^{143} (fig. S2). Again, this implies that this is the most likely place for the inner helices to bend. This conclusion is supported by blocker accessibility studies of inner helical cysteine mutants (*28*). It does not mean that all potassium channels bend at the equivalent position of Gly^{143} in KirBac1.1; it is likely that a

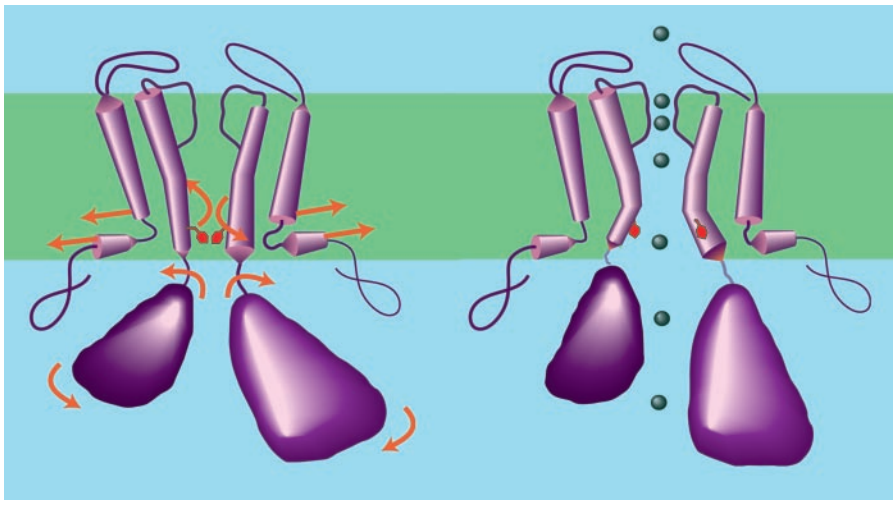

Fig. 6. Hypothetical gating mechanism for Kir channels. Schematic views of KirBac1.1 in the closed (**left**) and open (**right**) states. Sections of the protein closer to the viewer are drawn larger. The green bar represents the membrane. Blocking Phe^{146} residues are colored red. Arrows indicate the potential direction in which the different structural elements move when the channel opens.

number of potential positions along the inner helix allow bending.

It is possible that the channel makes use of both Gly^{134} and Gly^{143} sites during gating, but we believe that Gly^{134} plays a minor role in gating and a more important role in protein packing in Kir channels. Hence, as the channel begins to open, the slide helix moves laterally. Strain is exerted on the bottom of the inner helix, resulting in distortion of the helix at the nearest weak point, Gly^{143}. The blocking residue side chain of Phe^{146} beneath Gly^{143} then moves away from the center of the ion-conduction pathway.

Coupling of gating domain to the blocking residue. All ion channels have an ion-conduction pathway and a gate. Features of the ion-conduction pathway determine the specificity and rate of ion conduction, whereas the gate functions as a switch, opening and closing the pore at the desired time. The section of the protein that detects a signal such as a change in voltage across the membrane or binding of a ligand must transmit the signal to the gate to produce a gating action. With KirBac1.1 there has to be a coupling mechanism between the blocking residues of the inner helices and the intracellular domains.

The amphipathic slide helix is well placed to play a central role in this coupling mechanism. When the C-terminal assembly receives a signal, it is likely to undergo a conformational change. Again the precise change is unknown, but a rotation centered within the C-terminal domain would be consistent with the KirBac1.1 model and the proposed MthK domain motion. Because the outer helix is directly connected to the slide helix, it must move in the same direction, thereby creating room for the inner helix to bend.

Summary. KirBac1.1 was crystallized in a closed state, whereas all other K^+ channel structures to date have been open. KirBac1.1 prevents ion conduction by (i) occluding the ion-conduction pathway with the use of hydrophobic phenylalanine side chains, (ii) misaligning pore helices, (iii) decreasing the volume of the central cavity, and (iv) altering the conformation of the selectivity filter. The structure provides a hypothesis for gating, involving intracellular domain movement, slide helix movement, and bending of the inner helix just above the blocking residue. In our view, many K^+ channels are likely to share a fundamentally similar mechanism of gating and coupling in which properties of the gating domains determine how and when the channel opens.

References and Notes

1. F. M. Ashcroft, *Ion Channels and Diseases* (Academic Press, New York, 2000).
2. B. Hille, *Ionic Channels of Excitable Membranes* (Sinauer, Sunderland, MA, 2001).
3. S. R. Durell, H. R. Guy, *BMC Evol. Biol.* **1**, 14 (2001).
4. Materials and Methods are available as supporting material on *Science* Online.
5. M. Nishida, R. MacKinnon, *Cell* **111**, 957 (2002).
6. D. A. Doyle *et al.*, *Science* **280**, 69 (1998).
7. D. M. Cortes, L. G. Cuello, E. Perozo, *J. Gen. Physiol.* **117**, 165 (2001).
8. D. L. Minor Jr., S. J. Masseling, Y. N. Jan, L. Y. Jan, *Cell* **96**, 879 (1999).
9. G. Loussouarn, E. N. Makhina, T. Rose, C. G. Nichols, *J. Biol. Chem.* **275**, 1137 (2000).
10. Z. Lu, R. MacKinnon, *Nature* **371**, 243 (1994).
11. B. A. Wible, M. Taglialatela, E. Ficker, A. M. Brown, *Nature* **371**, 246 (1994).
12. Y. Kubo, Y. Murata, *J. Physiol.* **531** (no. 3), 645 (2001).
13. J. Yang, Y. N. Jan, L. Y. Jan, *Neuron* **14**, 1047 (1995).
14. M. Taglialatela, E. Ficker, B. A. Wible, A. M. Brown, *EMBO J.* **14**, 5532 (1995).
15. K. Imoto *et al.*, *Nature* **335**, 645 (1988).
16. A. N. Lopatin, E. N. Makhina, C. G. Nichols, *Nature* **372**, 366 (1994).
17. B. Fakler *et al.*, *FEBS Lett.* **356**, 199 (1994).
18. E. Ficker, M. Taglialatela, B. A. Wible, C. M. Henley, A. M. Brown, *Science* **266**, 1068 (1994).
19. S.-C. Tam, R. J. P. Williams, *J. Chem. Soc., Faraday Trans. 1* **80**, 2255 (1983).
20. N. Unwin, *J. Mol. Biol.* **229**, 1101 (1993).
21. N. Unwin, *Nature* **373**, 37 (1995).
22. G. Chang, R. H. Spencer, A. T. Lee, M. T. Barclay, D. C. Rees, *Science* **282**, 2220 (1998).
23. O. Beckstein, P. C. Biggins, M. S. P. Sansom, *J. Phys. Chem. B* **105**, 12902 (2001).
24. B. Roux, R. MacKinnon, *Science* **285**, 100 (1999).
25. Y. Zhou, J. Morais-Cabral, A. Kaufman, R. MacKinnon, *Nature* **414**, 43 (2001).
26. J. N. Bright, I. H. Shrivastava, F. S. Cordes, M. S. P. Sansom, *Biopolymers* **64**, 303 (2002).
27. Y. Jiang *et al.*, *Nature* **417**, 523 (2002).
28. D. del Camino, M. Holmgren, Y. Liu, G. Yellen, *Nature* **403**, 321 (2000).
29. Aesop; M. E. M. Noble, University of Oxford.

30. We thank the staff of the European Synchrotron Radiation Facility for help with data collection, including E. Gordon, J. McCarthy, S. Monaco, and S. Kozieiski. D.A.D. is grateful for support and helpful discussions from L. Johnson, M. Sansom, B. Guy, B. Wallace, L. Hong, S. Iwata, and M. Noble. J.M.G. thanks P. Colman and B. Smith. F.M.A. is funded by the Wellcome Trust and Medical Research Council. J.M.G. was funded by an International Senior Fellowship of the Wellcome Trust and by Australian National Health and Medical Research Council grant 257528. This work was funded by a Wellcome Trust Research Career Development Fellowship awarded to D.A.D. Coordinates for the KirBac1.1 structure have been deposited with the Protein Data Bank (accession code 1P7B; ID no. RCSB019097).

Supporting Online Material

www.sciencemag.org/cgi/content/full/1085028/DC1
Materials and Methods
Figs. S1 and S2
References

27 March 2003; accepted 29 April 2003
Published online 8 May 2003;
10.1126/science.1085028
Include this information when citing this paper.

REPORTS

Asteroseismology of HD 129929: Core Overshooting and Nonrigid Rotation

C. Aerts,[1]* A. Thoul,[2] J. Daszyńska,[1,3] R. Scuflaire,[2] C. Waelkens,[1] M. A. Dupret,[2] E. Niemczura,[3] A. Noels[2]

We have gathered and analyzed 1493 high-quality multicolor Geneva photometric data taken over 21 years of the B3V star HD 129929. We detect six frequencies, among which appear the effects of rotational splitting with a spacing of ~0.0121 cycles per day, which implies that the star rotates very slowly. A nonadiabatic analysis of the oscillations allows us to constrain the metallicity of the star to $Z \in [0.017,0.022]$, which agrees with a similar range derived from spectroscopic data. We provide evidence for the occurrence of core convective overshooting in the star, with $\alpha_{ov} = 0.10 \pm 0.05$, and we rule out rigid rotation.

Stars are composed of multiple gas layers with different temperatures, pressures, and chemical compositions. During their main-sequence phase, that is, while they transform hydrogen into helium in their core, a number of massive stars undergo oscillations. Through the study of these oscillations, scientists have a unique opportunity to probe the structure of specific layers of those stars. This type of investigation is termed asteroseismology. Here, we used asteroseismology to study the interior structure of a 10–solar mass ($M_\odot$) star of spectral type B, HD 129929. Such a massive B star has a well-developed convective core, the extension of which is uncertain because it depends on a poorly known phenomenon called core overshooting (inertial mixing of material from the convective core to the convectively stable upper layer). Moreover, the rotation of the star may be a source of mixing between the core and the outer layers. Both effects, which are in general difficult to disentangle from each other (*1*), affect the evolutionary path of the star; that is, they determine the way in which the star evolves to its supernova stage. In the case of HD 129929, we sought to determine the ef-